SLAC-PUB-11041
ATF Report–04-10, LBNL–57047, CBP Tech Note–333

Initial Studies of Nonlinear Dynamics in the KEK-ATF Wigglers*

A. Wolski†
Lawrence Berkeley National Laboratory, Berkeley, CA 94720

J. Nelson, M.C. Ross, M.D. Woodley
SLAC, Menlo Park, CA 94025

(Dated: **DRAFT:** February 23, 2005)

The nonlinear fields in insertion devices can have a significant impact on the beam dynamics in storage rings. Various tools have been developed which allow the dynamical effects of a wiggler to be predicted, based on a detailed model of the magnetic field. The wigglers in the KEK-ATF have recently been commissioned, and provide an opportunity for benchmarking some of the analysis tools. We report on initial studies of the nonlinear effects of the KEK-ATF wigglers, based on studies of the change in betatron tunes with change in orbit through the wigglers, and compare the results with the predictions based on detailed field models.

I. INTRODUCTION

The nonlinear fields in insertion devices can have a significant impact on the beam dynamics in storage rings. In some cases, it has been necessary to install additional magnets to compensate the more severe effects [1]. The effects of the wigglers in the damping rings for a future linear collider are of particular concern for three reasons. First, present designs require a high-field wiggler with total length much greater than usually found in storage rings (more than 400 m in some designs [2]). Second, the injected positron beam will have a very large emittance, and the effects of fields at large amplitudes from the magnetic axis can be expected to be significant. Third, the average injected beam power will be very large (of the order of 200 kW), and any particle losses from limited dynamic acceptance could cause serious operational problems.

Various tools are available for predicting the dynamical effects of a wiggler, based on a detailed field map. In one possible approach [3], the wiggler field is decomposed into a set of transverse and longitudinal modes; the mode representation allows the construction of a dynamical map in analytical form (e.g. as a Taylor series, or the generator of a Lie transformation); finally, the dynamical map can be used in a tracking code to study the effect of the wiggler on the dynamics. This procedure allows a judgement to be made as to whether the quality of the wiggler field is sufficiently good, or whether design modifications need to be made, e.g. shaping or widening the poles to reduce the field roll-off in the transverse direction. Starting from an idealized model of the wiggler field, the analysis is capable of determining the systematic effects of the wiggler; however, there are also random effects from construction tolerances, which may not be accurately known. There are also a variety of technical issues, including the challenge of obtaining a good fit to the field map. For these reasons, it is important to benchmark the analysis tools in as many cases as possible.

Four wigglers have recently been commissioned in the KEK-ATF damping ring test facility. The KEK-ATF is a 1.28 GeV storage ring with circumference 138 m. The wigglers are electromagnetic, with a 400 mm period, a gap of 20 mm and a peak field around 1.3 T. Each wiggler has 9 poles, plus two half-length poles at the entrance and exit, giving a total length of 2 m (measuring between the outside faces of the end poles). They are arranged in pairs, with one pair in the north straight, and the other in the south straight. In operation, the wigglers reduce the damping times (horizontal, vertical and longitudinal) from (17.0 ms, 28.5 ms, 21.5 ms) to (13.8 ms, 20.5 ms, 13.5 ms); the natural emittance is reduced from a little over 1.1 nm to a little below 1.0 nm. Design specifications of the wigglers are available that allow the construction of a detailed field model, suitable for an analysis of the effect on the beam dynamics as described above. In Section II we describe a field model for the wigglers calculated using the code RADIA [4]. In Section III we outline the construction of a dynamical model based on the detailed field map. Finally, in Section IV we compare some predictions of the dynamical model with experimental data that were recently obtained.

II. WIGGLER FIELD MODEL

A model of the KEK-ATF wigglers was constructed in the magnet modeling code RADIA, using the geometry shown in Fig. 1 [5].

The model is constructed with blocks and current-carrying coils, with the geometry of the blocks and coils, and the magnetic properties of the blocks specified. When the field is calculated, each block acquires a magnetization that is uniform within its volume, so the accuracy of the final field map depends on dividing the steel into sufficiently small blocks. However, the amount of computer memory needed for the field computation

*This work was supported by the Director, Office of Science, High Energy Physics, U.S. Department of Energy under Contract No. DE-AC03-76SF00098.
†Electronic address: awolski@lbl.gov

Work supported in part by the Department of Energy contract DE-AC02-76SF00515
SLAC, Stanford University, Stanford, CA 94309

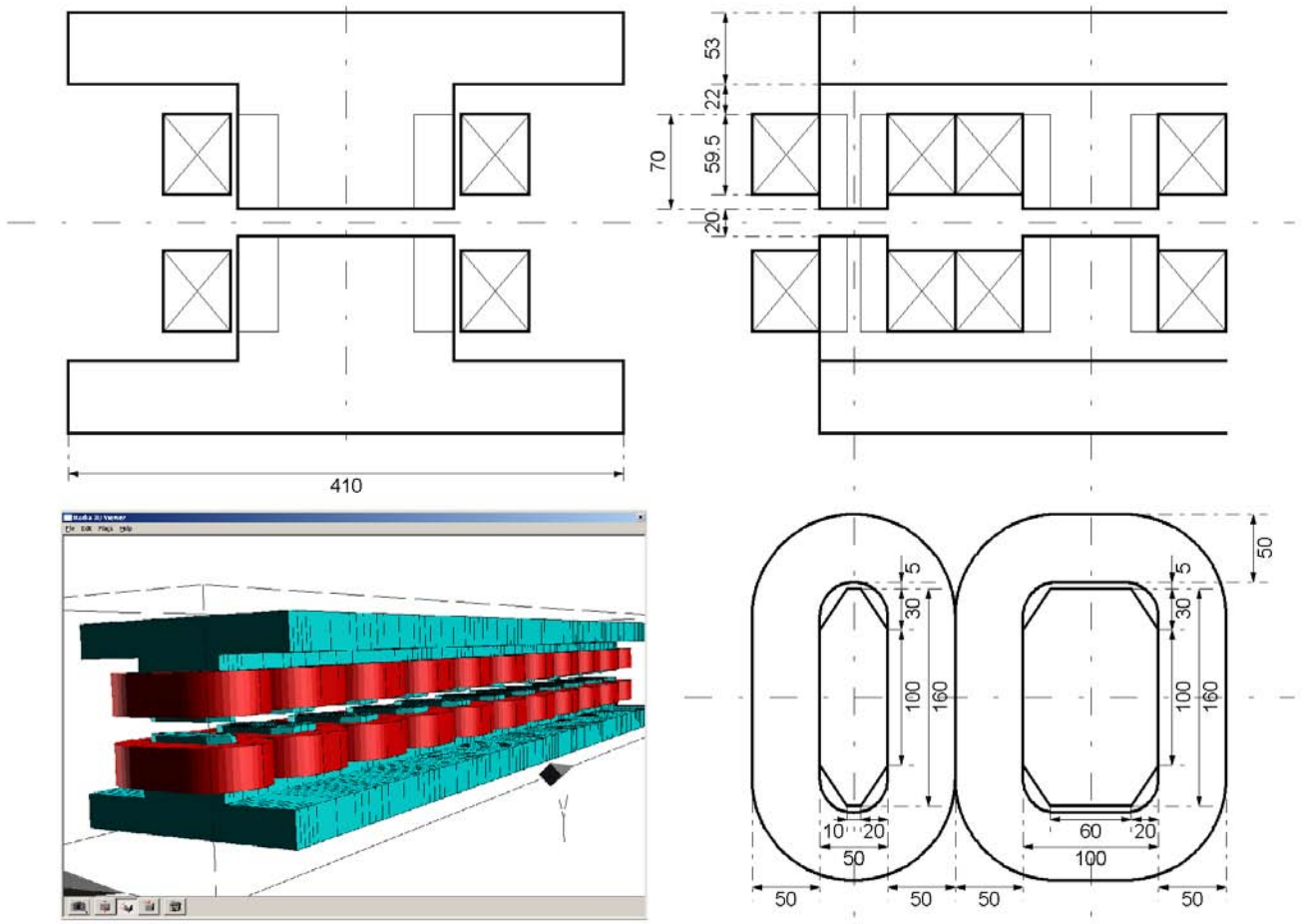

FIG. 1: Geometry of the KEK-ATF wigglers. Clockwise from top left: front elevation; side elevation, showing an end-pole and the adjacent full-length pole; cross-sections of an end-pole and the adjacent full-length pole; full wiggler model in RADIA. All dimensions are in mm.

increases rapidly as the number of blocks increases, and some compromises need to be made in defining the model. We are particularly interested in the transverse roll-off of the field, which is responsible for the horizontal focusing, and some of the nonlinear effects (including the dynamic octupole). We therefore use a relatively fine division (2.5 mm) of the blocks in the transverse horizontal direction, and keep the memory usage within limits by dividing the blocks less finely (12 mm) in the longitudinal direction.

The blocks are assumed to be composed of magnetic nonlinear, isotropic material; the magnetic properties are specified in terms of partial susceptibilities and saturations. The values used in the model of the KEK-ATF wigglers have been chosen to give the correct dependence of peak field on current. In particular, at the nominal operating current of 600 A, the peak field on-axis in the wiggler model is 1.36 T.

Modifications were made recently to the ends of each wiggler to correct steering effects. As we do not at present have a detailed description of the changes that were made, they were not included in our model. For this reason, we concentrate on the field map in the body of each wiggler, assumed to be perfectly periodic. The end effects may be significant, and will require more detailed future studies.

III. MODEL OF DYNAMICAL EFFECTS

Analysis of the dynamical effects of the wigglers proceeds in three steps:

- An analytic series is fitted to the detailed field map produced from the wiggler model.
- A differential algebra code is used to track through the field defined in terms of the analytic series. This step produces a dynamical map in Taylor form.
- The dynamical map is used in a tracking code to

simulate the dynamics in the storage ring with the wigglers turned on.

We consider each of these steps in turn. It should be noted that we assumed the field in the wiggler is truly periodic, so our map will represent the dynamics through each full period of the wiggler. In our lattice model, the end poles (and half of each adjacent full-width pole) will be represented by linear elements. Our assumption is valid if the nonlinear effects from the ends of the wigglers are small compared to the effects from the central portions. Accurate modeling of the ends of the wigglers requires some development of the tools that we presently have available; this work will be completed at a later date, and a more thorough analysis of the KEK-ATF wigglers will then be possible.

A. Analytic Fit to Numerical Field Map

The magnetic field components in a periodic section of a wiggler can be written in cylindrical polar co-ordinates as:

$$B_\rho = \sum_{m,n} \alpha_{mn} \mathrm{I}'_m(nk_z\rho)\sin(m\phi)\cos(nk_z z) \quad (1a)$$

$$B_\phi = \sum_{m,n} \alpha_{mn} \frac{m}{nk_z\rho} \mathrm{I}_m(nk_z\rho)\cos(m\phi)\cos(nk_z z) \quad (1b)$$

$$B_z = -\sum_{m,n} \alpha_{mn} \mathrm{I}_m(nk_z\rho)\sin(m\phi)\sin(nk_z z) \quad (1c)$$

Here, $\mathrm{I}_m(x)$ are modified Bessel functions, and $k_z = 2\pi/\lambda_w$ where λ_w is the wiggler period. The coefficients α_{mn} for a particular field may be found from a two-dimensional Fourier analysis of the radial field component (1a) on a cylinder centered on the magnetic axis of the wiggler (i.e. a surface with a fixed value of ρ). The radius of the cylinder is, in principle, arbitrary. However, because of the radial dependence of the field, the residuals of the fit diverge exponentially outside the cylinder, and converge towards the axis. It is therefore desirable to choose a cylinder with a large radius, with the restriction that the original field calculation sometimes lacks accuracy close to the pole tips. In the present case, we have used a cylinder of radius 7 mm (the half-gap of the wiggler is 10 mm). Experimentally, we were able to move the orbit ±4 mm in the wigglers, so a cylinder of 7 mm is more than sufficient for our purposes.

We obtained a good fit to the numerical field map using 175 modes, with mode numbers up to 9 radially and 69 longitudinally. The variation of the vertical field component in the transverse and longitudinal directions is shown in Fig. 2. The residuals of the vertical field component are shown on the mid-plane, and on a horizontal plane 6 mm above the mid-plane, in Fig. 3. On the mid-plane, the error in the fit is a fraction of a Gauss. Note that given the vertical field component on the mid-plane, all field components throughout the wiggler are constrained by Maxwell's equations, and can be reconstructed using Eqns. (1).

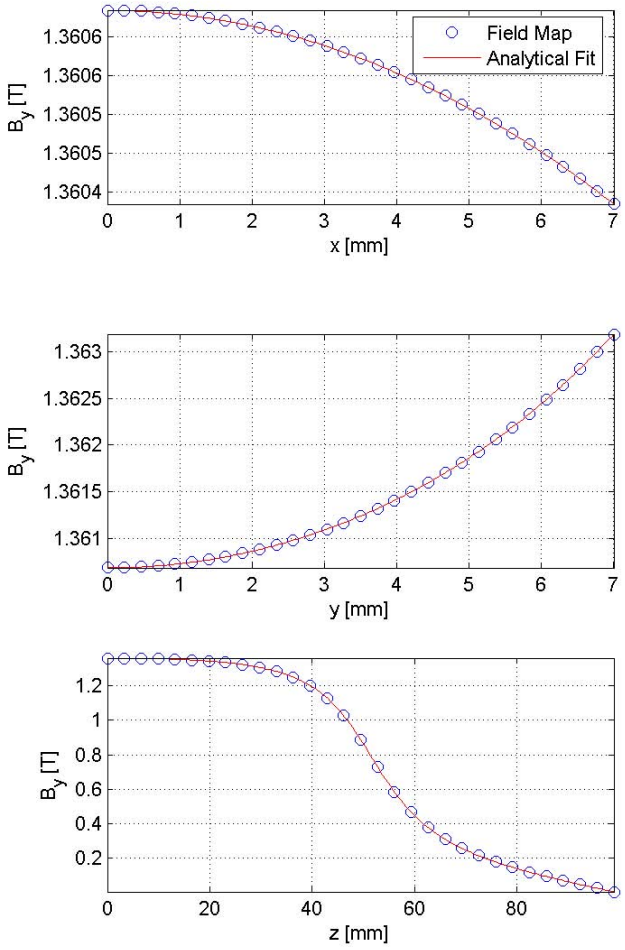

FIG. 2: Variation of vertical field component in the KEK-ATF wigglers. Top: variation with transverse horizontal co-ordinate. Middle: variation with vertical co-ordinate. Bottom: variation with longitudinal co-ordinate through one quarter period of the wiggler. The blue circles indicate values from the numerical field map generated in RADIA, and the red lines show the field reconstructed from the analytic fit.

B. Construction of the Dynamical Map

Having obtained an analytic expression for the magnetic field in the wiggler, we use the differential algebra code COSY [6] to produce a dynamical map by integrating through the field. The order of the map produced is limited only by the processor time taken to calculate the map; we calculate maps that include terms up to

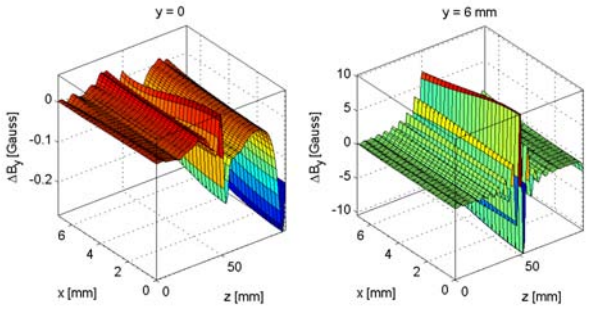

FIG. 3: Residuals of analytic fit to numerical field data in the KEK-ATF wigglers. Left: residuals on the mid-plane. Right: residuals on a horizontal plane 6 mm above the mid-plane.

fifth order. The dynamical map is in the form of Taylor series in the dynamical variables. COSY includes a Runge-Kutta routine for integrating the equations of motion of a relativistic particle in a magnetic field, but the resulting map is not constrained by symplecticity. We therefore compare the results of the Runge-Kutta integration with those of an explicit symplectic integrator [7] available for use with COSY. The explicit symplectic integrator produces a map that is symplectic up to a given order. The disadvantage with the explicit symplectic integrator is that the paraxial approximation needs to be made in the equations of motion, so some terms in the map are underestimated.

A comparison between the map produced by the Runge-Kutta integrator and that produced by the explicit symplectic integrator is shown in Fig. 4. There is close agreement between the two integration methods, except for those terms that are omitted in the paraxial approximation made in the explicit symplectic integrator.

The symplecticity of a map may be verified by calculating the Jacobian J of the map algebraically, and constructing $Z = J^{\mathrm{T}} \cdot S \cdot J - S$, where S is the usual antisymmetric form. A symplectic map will satisfy $Z = 0$. For a map that is symplectic to order n, only terms of order n and higher will occur in Z. We can then estimate the symplectic error in a map by looking at the coefficients of terms of different order in Z. A comparison between the maps produced by Runge-Kutta integration and the explicit symplectic integrator is shown in Fig. 5.

We see that for both maps, the errors in the low order terms are generally small; for higher-order terms, the errors in the map produced using the explicit symplectic integrator are nearly two orders of magnitude smaller than the errors in the map produced using the Runge-Kutta integrator. In fact, the symplectic error in the map from either integrator is small enough not to be significant for the present studies, and both maps produce

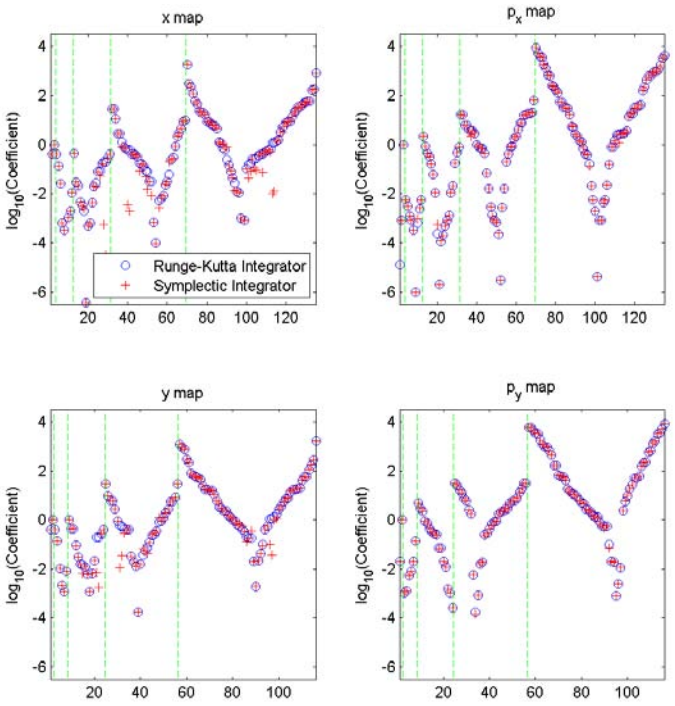

FIG. 4: Coefficients of terms in the Taylor series maps through one period of the KEK-ATF wigglers. Only the maps for the transverse variables are shown, but the full map includes the longitudinal variables. The coefficients of terms of different orders are grouped together and separated by the vertical green broken lines. The maps include terms up to fifth order.

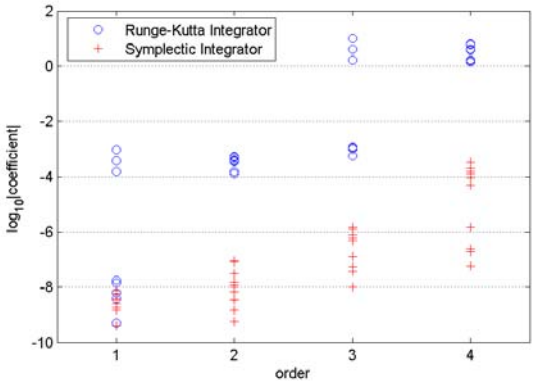

FIG. 5: Coefficients of terms in $Z = J^{\mathrm{T}} \cdot S \cdot J - S$, grouped according to the order of the term.

essentially the same results.

The closed orbit through one wiggler period, calculated using the symplectic integrator in COSY, is shown in Fig. 6. Note that the design of the ends of the wigglers leads to a trajectory that lies entirely to one side of the wiggler axis. The amplitude $\hat{x}$ of the orbit oscillation may be

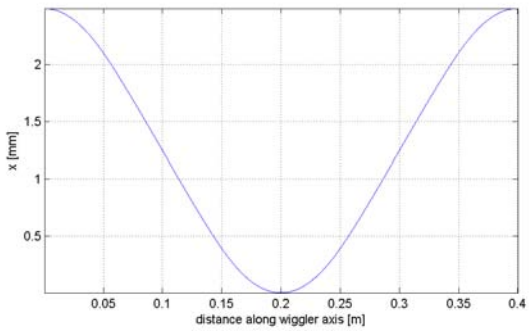

FIG. 6: Closed orbit through one period of a wiggler, calculated using the symplectic integrator in COSY.

estimated from a sinusoidal model for the wiggler field:

$$\hat{x} = \frac{\hat{B}}{B\rho k_z^2} \tag{2}$$

where $\hat{B}$ is the peak wiggler field, $B\rho$ is the beam rigidity, and $k_z = 2\pi/\lambda_w$ where λ_w is the wiggler period. For a beam energy of 1.28 GeV, a wiggler peak field of 1.36 T, and a wiggler period of 0.4 m, the expected amplitude of the orbit oscillation is 1.29 mm, or 2.58 mm peak-to-peak. This is in good agreement with the COSY calculation.

The linear focusing from one wiggler period may be estimated from the coefficients R_{21} and R_{43}, for the horizontal and vertical planes respectively. The horizontal focusing is principally a result of the sextupole component of the wiggler poles, which feeds-down to a linear focusing component as a result of the oscillation of the closed orbit through the wiggler. The vertical focusing is principally a result of the closed orbit crossing the longitudinal fringe-fields of the poles at an angle. From both the symplectic integrator and the Runge-Kutta integrator in COSY, we obtain values $R_{21} = 8.56 \times 10^{-4}$ m^{-1} and $R_{43} = -2.00 \times 10^{-2}$ m^{-1}. We can compare these values with those obtained by fitting the focusing in a lattice model to give the measured tunes. For this comparison, we determined the strengths of the main multipoles in the model from the settings in the machine, and then adjusted the edge focusing and quadrupole focusing in the wigglers to give the correct tunes. From this "empirical linear model" we obtained the values $R_{21} = 25.1 \times 10^{-4}$ m^{-1} and $R_{43} = -1.93 \times 10^{-2}$ m^{-1}. In relative terms, the vertical focusing from the COSY integration agrees well with the empirical model, but the horizontal focusing is about a factor of 3 too small. In absolute terms, the error in both cases is of the order 10^{-3} m^{-1}. Although the absolute focusing error is fairly small, better agreement between the two models is desired. The reason for the discrepancy is unclear. It is likely that the field in the RADIA model does not accurately represent the field in the actual wigglers, or the end effects (which have not been properly included) are somewhat stronger than might be expected. It is also possible that the empirical linear model of the wigglers is not accurate, and that the focusing effects included in the wigglers to match the tunes in the machine are compensating for errors elsewhere in the model. The tune error from the difference in the horizontal focusing between the two models, is given by:

$$\Delta\nu_x = \frac{1}{4\pi}\bar{\beta}_x \Delta R_{21} N_\lambda \tag{3}$$

where $\bar{\beta}_x \approx 8$ m is the average horizontal beta function in the wigglers, and $N_\lambda = 20$ is the total number of periods in the four wigglers. With $\Delta R_{21} \approx 16 \times 10^{-4}$ m^{-1}, we find $\Delta\nu_x \approx 0.021$; a small but significant tune error.

The oscillation in the closed orbit through the wiggler leads to a feed-down of the decapole component in the wiggler poles to give a "dynamic octupole" component in the map. From Fig. 4 we see that the coefficients of the third order terms in the map are of order 1 or less. This suggests that the nonlinear effects from the wigglers will be very small. Specifically, the dynamic octupole component is characterized by the coefficient of the x^3 term in the map for p_x; this is around 0.8 m^{-3}. This means that a particle with a 1 mm horizontal offset will receive a horizontal kick of less than 10^{-9} radians from this term in traversing one wiggler period. The small nonlinear effects are emphasized by inspection of the transfer functions, shown in Fig. 7. The deviations from a linear relationship between initial transverse offset and resulting transverse kick are very small. Also plotted in Fig. 7 are the linear focusing from the empirical linear model, showing good agreement in the vertical plane, but a factor of 3 difference in the horizontal plane. Where the sextupole component in the wiggler poles is small, as in the present case, the vertical focusing is generally much stronger than the horizontal.

C. Simulations of Effects of KEK-ATF Wigglers on Beam Dynamics

We used the maps produced by COSY to simulate the impact of the KEK-ATF wigglers on the chromaticity, and on the change of betatron tune with horizontal orbit bump through the wigglers. Here, we outline the procedures used in the simulations.

We constructed three lattice models for comparison with experimental data:

- **Model A** is a lattice model with the wigglers off. The magnet strengths are determined from the machine settings at the time the measurements (with wigglers off) were made. Small changes (around 2%) were made to the sextupole strengths in the model to fit the measured chromaticity.

- **Model B** is a lattice model with the wigglers on. The wigglers are represented by linear elements. The magnet strengths were taken from the time the measurements (with wigglers on) were made. The

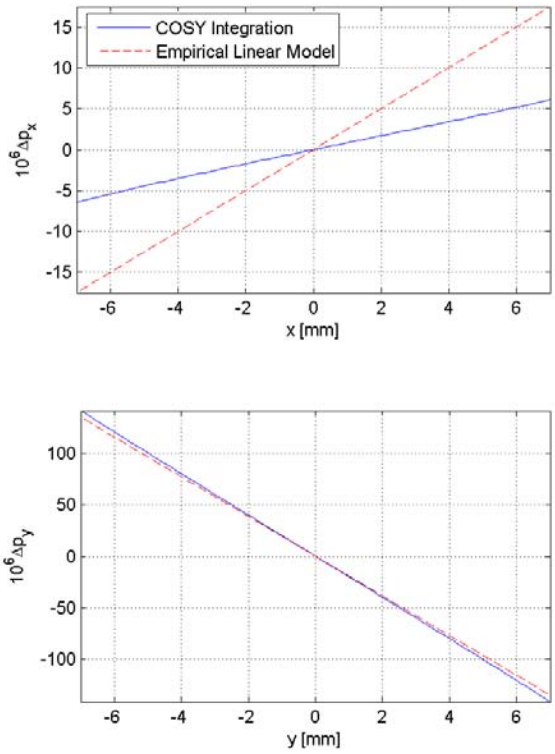

FIG. 7: Transfer functions showing the transverse kicks received as a function of initial transverse offset for a particle passing through one period of the KEK-ATF wigglers. Top: horizontal transfer function. Bottom: vertical transfer function. The solid blue lines show the transfer functions from a fifth-order Taylor map calculated using a symplectic integrator in COSY; the broken red lines show the focusing in a linear model fitted to the observed machine tunes.

parameters of the wigglers were adjusted (by including small quadrupole focusing and dipole edge focusing effects) to reproduce the measured betatron tunes. The same scaling factors for the sextupoles as in Model A were applied.

- **Model C** is identical to Model B, except that each full period within each wiggler is represented by a fifth-order Taylor map. The Taylor map was produced by the explicit symplectic integrator. The ends of the wiggler are the same as in Model B.

Simulations were carried out using the tracking code MERLIN [8]. For each model, we calculated the variation in betatron tunes with energy. Horizontal orbit bumps were calculated for each of the two pairs of wigglers, using four orbit correctors for each wiggler pair. The bumps were found to close correctly in both the model and the machine. Since the orbit varies slightly through the wigglers, the amplitude of the bump was defined to be the horizontal offset at the BPM between the two wigglers in a given pair. A range of bump settings over ± 5 mm were applied in the model, and for each bump setting, the tunes were calculated from the eigenvalues of the single-turn transfer matrix around the closed orbit.

IV. EXPERIMENTAL RESULTS

Fig. 8 shows the chromaticity in the KEK-ATF with the wiggler off. Magnet strengths for the model were taken directly from the machine settings, with a correction of the order of 2% in the sextupoles to match the measured chromaticity. Fig. 9 shows the chromaticity with wigglers on. The same correction factor was applied to the sextupoles as in the case with wigglers off. With the wigglers on, the measured chromaticity appears to be significantly different from the chromaticity in the model; however, the chromaticities in this case are extremely small, and the horizontal tune shifts being measured are of the order 10^{-3}. In this regime, even small errors in the model may appear to have significant impact. We note, however, that the fit to the data in Fig. 9 from the nonlinear wiggler model is a little better than that from the linear wiggler model.

The only magnets within the orbit bumps (apart from the wigglers themselves) are quadrupoles and correctors. With the wigglers off, there are four possible sources of tune variation with orbit bump: chromatic effects; edge focusing from the corrector magnets; higher-order multipoles in the quadrupoles and correctors; and residual closed-orbit distortion outside the orbit bump. The first two effects are systematic, and are included in the models. The last two effects are the result of random errors that are not well characterized, and are not included in the models. We can judge the likely signficance of each of these effects, by estimating the parameters necessary to produce a tune change of 10^{-3} with a horizontal orbit bump of 4 mm. This magnitude of tune change corresponds roughly to the observed effects.

Chromatic effects. The bump causes a change in the circumference, which leads to a small change in the beam energy, which in turn causes a change in the betatron tunes because of the chromaticity. As the first two (and last two) corrector magnets used in the bumps are roughly Δs =3 m apart, a bump Δx =4 mm through one pair of wigglers causes a change in circumference of the order $\Delta x^2/\Delta s \approx 5$ μm. Since the nominal circumference is 138 m, and the momentum compaction is 2.1×10^{-3}, the energy change resulting from a change in circumference of 8 μm is roughly $\Delta p/p \approx 2\times10^{-5}$. To give a tune change of 10^{-3}, a chromaticity of the order of 50 would be needed. The measured chromaticities are of order 1, so chromatic effects resulting from the orbit bumps in the wigglers are small.

Edge focusing from the corrector magnets. With a 3 m separation between the corrector magnets, the angular kick needed to give a 4 mm bump is $\Delta\theta$ =1.3 mrad.

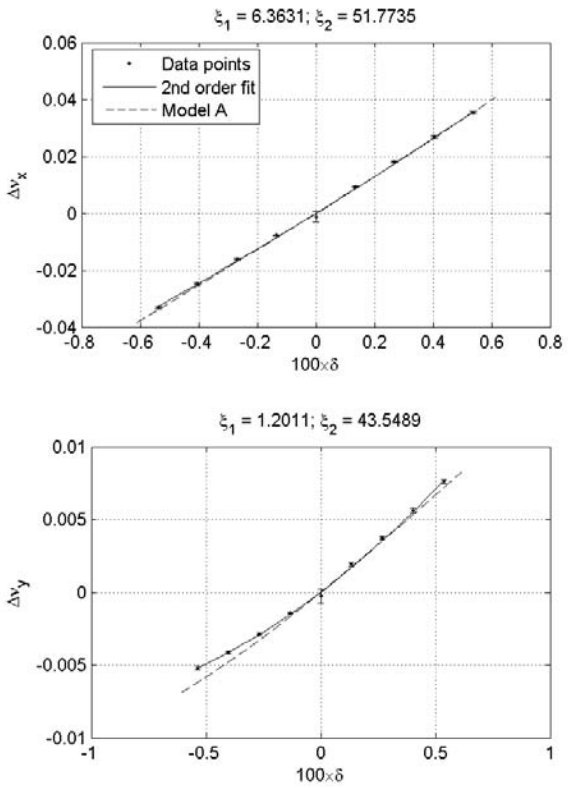

FIG. 8: Chromaticity with wigglers off. ξ_1 is the linear chromaticity fitted to the data points; ξ_2 is the second-order chromaticity.

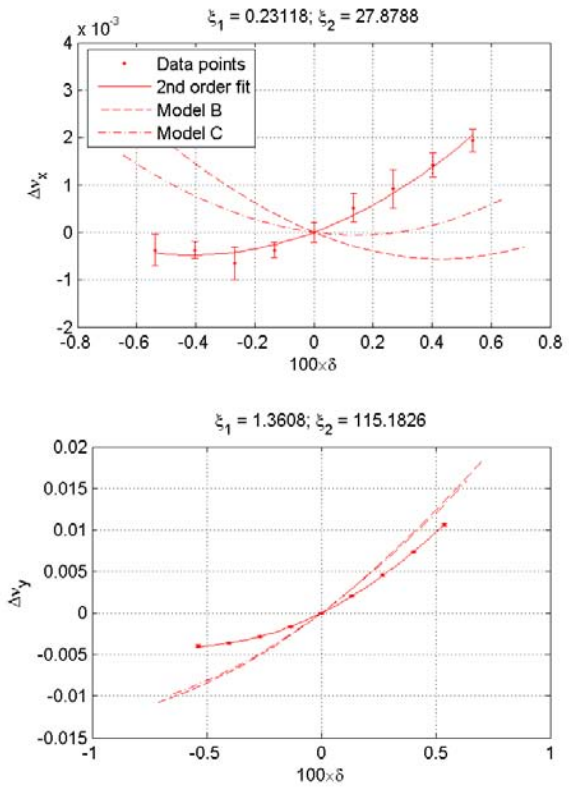

FIG. 9: Chromaticity with wigglers on. ξ_1 is the linear chromaticity fitted to the data points; ξ_2 is the second-order chromaticity.

The edge focusing from the corrector magnets is of the order $\Delta k_1 l = h \tan\psi$, where $h = 1/\rho = \Delta\theta/L$ for a bending radius of ρ in a corrector magnet of length L, and $\psi \approx \Delta\theta$ is the orbit angle with respect to the pole-face of a corrector. As the corrector magnets are 6 cm long, for a 4 mm bump, the focusing is roughly $\Delta k_1 l \approx 3 \times 10^{-5}$ m^{-1}. With a typical beta function in the correctors of 5 m, the change in tune is roughly $\Delta\nu \approx (1/4\pi)\beta\Delta k_1 l \approx 10^{-5}$. In the horizontal plane, since the edge effects of the corrector magnets are defocusing, a reduction in tune is expected. The tune change is quadratic in the bump amplitude, because of the dependence of the focusing on both the orbit angle with respect to the corrector pole face, and the strength of the corrector.

Higher-order multipoles in the quadrupoles and correctors. Sextupole components in the quadrupoles will cause linear changes in tune with the size of the orbit bump; octupole components will cause quadratic changes in tune with the size of the orbit bump. If a corrector magnet at the center of the bump contains a sextupole component with strength proportional to the strength of the corrector, then this will result in quadratic changes in tune with the size of the orbit bump. With an integrated sextupole strength $k_2 l$, the linear focusing from an orbit bump of Δx will be $\Delta x k_2 l$, and the tune change will be $\Delta\nu \approx (1/4\pi)\beta\Delta x\Delta k_2 l$. To give a tune change of 10^{-3} with an orbit bump of 4 mm, an integrated sextupole component of roughly 0.6 m^{-2} is needed. At a reference radius r, a sextupole component k_2 gives a field strength $B\rho k_2 r^2/2$. Therefore, with a corrector length of 6 cm, an integrated sextupole component $0.6m^{-2}$ gives a field strength of a little under 0.01 T at a reference radius of 2 cm. The corrector dipole field with an orbit bump of 4 mm is roughly 0.1 T. This means that with an orbit bump of 4 mm, the sextupole field component needs to be around 10% of the dipole field component to give a tune shift of 10^{-3}.

Residual closed-orbit distortion outside the orbit bump. Small changes in horizontal orbit around the ring will cause linear changes in horizontal and vertical tune with changes in the size of the orbit bump, because of changes in the horizontal offset of the beam with respect to the centers of the sextupoles. A rough estimate of the tune change that might be expected from a closed orbit distortion (uncorrelated with the sextupole positions) with rms σ_x is given by $\Delta\nu \approx \sqrt{N_{sext}}\beta k_2 l\sigma_x/4\pi$, where $N_{sext} = 68$ is the number of sextupoles in the ring. With a beta function of 5 m, and an integrated sextupole

strength $k_2 l \approx 30$ m^{-2}, a tune change of 10^{-3} will result from a closed orbit distortion with rms 10 μm.

The chromatic and edge focusing effects are expected to be small. The random effects, particularly the closed orbit distortion, may be significant.

Fig. 10 shows the variation of the tunes with orbit bump in the north wigglers, with wigglers on and wigglers off. Fig. 11 shows the variation of the tunes with orbit bump in the south wigglers, with wigglers on and wigglers off. Results from the three models are plotted on the same axes as the experimental data. Note that we suppress differences in tunes when the bumps are turned off, by plotting the tune change with respect to the zero-bump value. The lattices used with the wigglers off are different from those with the wigglers on and have slightly different tunes. Also, as discussed in Section III B, the focusing obtained from integrating through the modeled wiggler field is slightly different from that needed to fit the tunes in the model to the measured tunes.

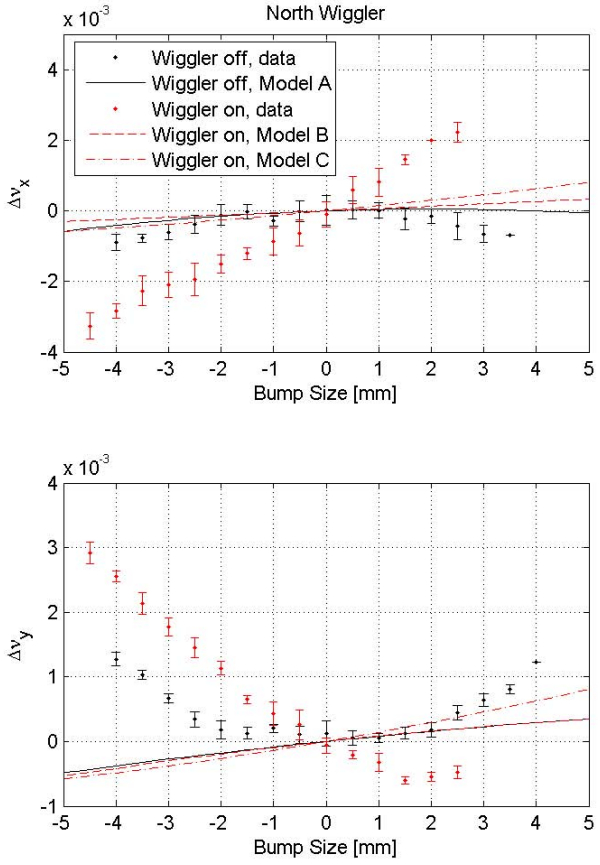

FIG. 10: Tune variations with orbit bump in the north wigglers. The model with the wiggler off is Model A; the linear wiggler model is Model B; the nonlinear wiggler model is model C.

The models do not fit the data particularly well. Even

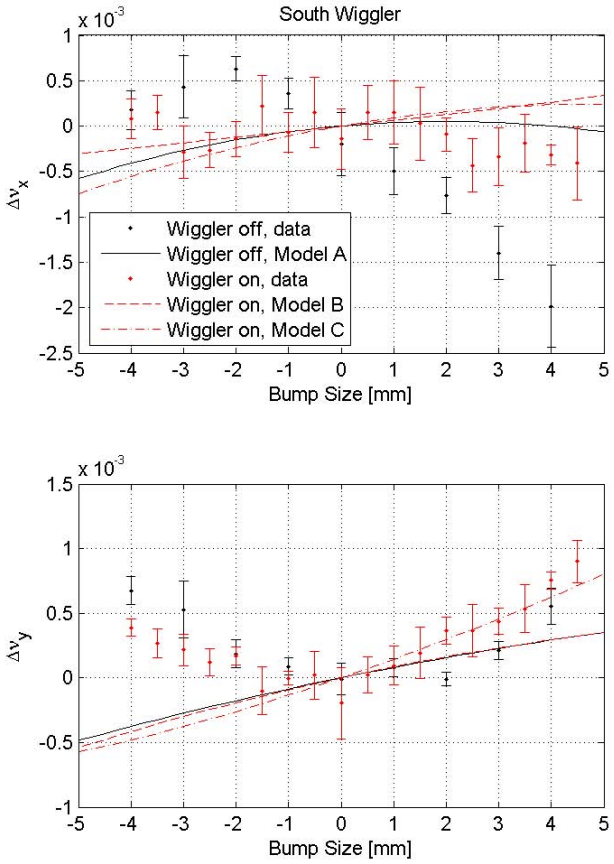

FIG. 11: Tune variations with orbit bump in the south wigglers. The model with the wiggler off is Model A; the linear wiggler model is Model B; the nonlinear wiggler model is model C.

with the wigglers off, we observe significantly larger tune changes with orbit bump than expected from the lattice model. However, as we discussed above, tune changes of the magnitudes observed may arise from multipole components in the corrector magnets of the order of a few % of the corrector dipole field, or from a residual closed orbit distortion of a few microns outside of the bump. As these effects are not well characterized, they have not been included in the models. From the models, we expect turning on the wigglers to have a relatively small effect on the tune variations with orbit bumps, compared with the effects of orbit distortions, for example. In the data we collected, it is not possible to separate the nonlinear effects of the wigglers from other effects causing changes in tune with with orbit bumps through the wigglers.

V. CONCLUSIONS

We have constructed a magnetic field map for the KEK-ATF wigglers, and have used this map to produce a model of the effects of these wigglers on the beam dynamics in the storage ring. The transverse profile of the field in the wigglers is rather flat, which means that the linear and nonlinear effects are weak. Beyond this, it is difficult to draw any clear, general conclusions from comparisons between the models and the measured data. The horizontal linear focusing does appear to be underestimated in the model, which suggests the transverse field roll-off could be a little larger than predicted from solving the magnetic model. There is reasonable agreement between the chromaticity in the models and the chromaticity measured in the machine, after making small (roughly 2%) adjustments to the sextupole strengths in the models.

We attempted to characterize the dynamic octupole effects in the wigglers by measuring the tune changes with orbit bumps; however, it appears that the results are dominated by other effects, possibly higher-order multipoles in the quadrupoles and steering magnets, or residual closed orbit distortions outside of the bumps. Other techniques for studying the nonlinear effects of the wigglers can be used which would allow a more precise analysis. For example, if one applies a kick to the bunch on a single turn and obtains the tunes as a function of kick amplitude using turn-by-turn BPMs, there should not be any effects from the closed orbit distortion, since the closed orbit is not changing.

It is also possible that there are significant effects from the ends of the wigglers, which have not been correctly described in the models. To determine these effects properly, models need to be constructed that include the recent modifications made to correct the steering effects of the ends.

Acknowledgements

We should like to thank our hosts at KEK during our visit, for invaluable support and assistance with this work.

[1] J. Safranek *et al.* "Nonlinear Dynamics in a SPEAR Wiggler," PRST-AB **5**, 010701 (2002).

[2] TESLA Technical Design Report, Chapter 5. DESY 2001-011 (2001).

[3] A. Wolski, M. Venturini, S. Marks, W. Wan, "Frequency Map Analysis of Nonlinear Dynamics in the NLC Main Damping Rings," LBNL-56505 (2004).

[4] O. Chubar, P. Elleaume, J. Chavanne, "A 3D Magnetostatics Computer Code for Instertion Devices," J. Synch. Rad. **5**, 481-484 (1998). `http://www.esrf.fr/Accelerators/Groups/InsertionDevices/Software/Radia`

[5] Thanks to J. Urakawa (KEK) for providing detailed engineering drawings of the wigglers.

[6] M. Berz *et al.* "COSY INFINITY and its Applications in Nonlinear Dynamics," in "Computational Differentiation: Techniques, Applications and Tools," SIAM (1996). `http://bt.pa.msu.edu/index_files/cosy.htm`

[7] Y.K. Wu, E. Forest, D.S. Robin, "Explicit Symplectic Integrator for s-Dependent Static Magnetic Field," Phys. Rev. E **68**, 046502 (2003).

[8] N.J. Walker, "MERLIN: A C++ Class Library for Performing Charged Particle Accelerator Simulations," `http://www.desy.de/~merlin/`